Peer-reviewed version available at Math. Comput. Appl. 2019, 24, 12; doi:10.3390/mca24010012

Article

Modeling the Effects of Macrophages on Bone Fracture Healing

Imelda Trejo [1,*], Hristo Kojouharov [1] and Benito Chen-Charpentier [1]

[1] Department of Mathematics, The University of Texas at Arlington, P.O. Box 19408, Arlington, TX 76019-0408, USA

* Correspondence: imelda.trejo@mavs.uta.edu; Tel.: +1-817-272-3261

Academic Editor: name
Version November 16, 2018 submitted to

Abstract: A new mathematical model is presented to study the effects of macrophages on the bone fracture healing process. The model consists of a system of nonlinear ordinary differential equations that represents the interactions among classically and alternatively activated macrophages, mesenchymal stem cells, osteoblasts, and pro- and anti-inflammatory cytokines. A qualitative analysis of the model is performed to determine the equilibria and their corresponding stability properties. Numerical simulations are also presented to support the theoretical results and to monitor the evolution of a broken bone for different types of fractures under various medical interventions. The model can be used to guide clinical experiments and to explore possible medical treatments that accelerate the bone fracture healing process either by surgical interventions or drug administrations.

Keywords: Bone repair, macrophages, immune system, cytokines, mesenchymal stem cells

1. Introduction

Bone fractures are becoming a big worldwide problem due to their high frequency and surgical complications. Globally, osteoporosis causes more than 8.9 million fractures every year affecting 50% of women and 25% of men over age 50 [1–3]. Furthermore, 10-15% of bone fractures do not heal or take longer to heal [4,5]. Surgical complications, disabilities, and high morbidity rates often occurs from severe traumas and immune-compromised-fractured people [1,5]. The most dangerous trauma is the hip fracture with mortality rates up to 20-24% in the first year after the fracture and greater risk of dying may persist for at least 5 years afterwards [6]. Traffic accidents, the number one killer of young people and the major causes of fractures, are expected to be one of the top three causes of disabilities by 2020 [7,8]. In addition, medical care costs for osteoporotic bone fractures are expected to be over US$25 billions by 2025; due, in part, to the expensive treatments and the prolonged hospitalization and rehabilitations [1,9]. It is essential to have a better understanding of the bone fracture healing process in order to prevent unsuccessful healing and to develop optimal fracture union treatments.

Although significant improvements have been made in the experimental and mathematical modeling of the bone fracture healing process over the last twenty years, however the optimal conditions for bone repair are still unclear [10–12]. Treatments based on anti-inflammatory cytokines, such as the cytokine-specific agents that block the pro-inflammatory cytokines productions, have exhibited promising clinical results and have led to intense orthopedic research activities [4,5,12–16].

Recently, a mathematical model based on the interactions among macrophages, mesenchymal stem cells (MSCs), and osteoblast was developed to study the regulatory effects of two generic pro- and anti-inflammatory cytokines during the early stages of bone fracture healing [17]. To our knowledge, it was the first attempt to incorporate the macrophages interactions in the modeling of the bone fracture healing process. The mathematical model revealed that high concentrations of pro-inflammatory cytokines negatively affect the healing time of a fracture and that the administration of anti-inflammatory cytokines can accelerate the healing time in a dose-dependent manner. However, the model assumed that the only source of anti-inflammatory cytokines is given by the MSCs, which

Peer-reviewed version available at Math. Comput. Appl. 2019, 24, 12; doi:10.3390/mca24010012

may not be enough to promote and correctly represent the complex pattern of bone fracture healing formation. Therefore, it is better to incorporate the other sources of anti-inflammatory cytokines during the bone fracture healing process, such as the delivered from the macrophages [1,5,18].

In this paper, the mathematical model developed in [17] is extended to separately incorporate the two different phenotypes of macrophages: classically and alternatively activated macrophages, as they have distinct functions during the tissue healing [18,19]. Classically activated macrophages release high levels of pro-inflammatory cytokines, including the TNF-α and IL-1β which exhibit inhibitory and destructive properties in high concentrations [13,19]. In contrast, alternatively activated macrophages are characterized with the secretion of the anti-inflammatory cytokines such as the IL-10 which increase their phagocytic activities, mitigate the inflammatory responses, promote growth and accelerate fracture healing [1,5,18,19]. This extension leads to a more realistic model by incorporating the different phagocytic rates and the separate production of the pro- and anti-inflammatory cytokines by the two types of macrophages [18,20]. The model can be used to investigate potential therapeutic treatments based on the use of anti-inflammatory cytokines, stem cells, and macrophages, suggesting possible ways to guide clinical experiments and bone tissue engineering strategies [18,19].

The organization of the paper is as follows: Section 2 discuses the cellular and molecular interactions that occur during the bone fracture healing process. The simplifying assumptions are presented in Section 3. In Section 4, a system of nonlinear ordinary differential equations is introduced to describe the fundamental aspects of the bone fracture healing process during the resolution of inflammation and bone repair. The stability analysis of the system is presented in Section 5. Section 6 demonstrates the functionality of the model by numerically simulating the progression of the bone fracture healing process under normal and pathological conditions. The discussion and future work are presented in Section 7.

2. Biological Background

Bone fracture healing is a complex regenerative process that involves the participation of different cell types including the immune system and mesenchymal lineage cells [21]. Their interactions and functions are strongly regulated by molecular and mechanical stimuli [19,22]. Particularly, at the beginning of the healing process, cytokines either have positive or negative effects on the cellular functions depending on the influence of other cytokines, concentration, and exposed time [23–25].

Cytokines are functionally classified into pro-inflammatory and anti-inflammatory families. Pro-inflammatory cytokines such as the tumor necrotic factor-α (TNF-α) activate the immune system defense to kill bacteria and fight infections, while anti-inflammatory cytokines inhibit pro-inflammatory synthesis and activate the mesenchymal lineage cellular functions [5]. The interleukin-10 (IL-10) is one of the most potent anti-inflammatory molecules that inhibit the pro-inflammatory production [5,26].

The pro-inflammatory cytokines concentration during the bone fracture healing process is mainly delivered by necroses of cells and by the inflammatory immune cells, such as monocytes and neutrophils, that arrive to the injury site in response to the trauma [4]. These pro-inflammatory profiles, which include the TNF-α, lead to an acute inflammation observed in the first 24 hrs [11,27,28] after injury. Monocytes migration mostly occurs during the beginning of the acute period, when monocytes also differentiate into macrophages to resolve the inflammation. Once this differentiation starts, the influx of the inflammatory cells ceases and they die out [29].

During the resolution of inflammation, macrophages increase their population by migration and they activate to their classical and alternative phenotypes accordingly to the cytokines stimuli [19,30]. The two phenotypes can also shift between each other during this process [31,32]. Macrophages have the capability to release both pro- and anti-inflammatory cytokines through their different activation [31]. Classically activated macrophages release high concentration of pro-inflammatory cytokines, such as the TNF-α, and low levels of anti-inflammatory cytokines [31] in responses to their engulfing functions. Alternative macrophages secrete high level of the Il-10 and low levels of TNF-α as they continue with the clearance of debris and the modulation of inflammation [31]. The correct balance of

Peer-reviewed version available at Math. Comput. Appl. 2019, 24, 12; doi:10.3390/mca24010012

TNF-α during bone repair is necessary for successful fracture healing. High levels of TNF-α induce a chronic inflammation and gradual destruction of cartilage and bone tissue [25], while the absence of TNF-α impairs fracture healing [13,15].

In addition, during the resolution of inflammation, MSCs arrive to the injury site, activate their immune-modulation functions by releasing the IL-10, and proliferate or differentiate into fibroblasts, chondrocytes, and osteoblasts [5,33]. Fibroblasts and chondrocytes proliferate and release the fibrinous/cartilagenous extracellular matrix, which fills up the fracture gap [33,34]. Osteoblast cells proliferate, synthesize the new woven bone, and differentiate into osteocytes or die out [22,33].

During the last stage of the bone fracture healing process, the fibrocartilage and the woven bone are constantly removed and replaced by a functional bone [35]. This process is referred to as bone remodeling and consists of a systematic tissue degradation and production by osteoclasts and osteoblasts, respectively. Bone remodeling is a slow process that can take months to years until the bone recovers to its pre-injury state [11].

The inflammation is considered resolved when debris are eliminated, activated macrophages emigrate to the lymphatic nods to die, and inactivated macrophages return to their normal density [29]. These evens are observed after two weeks from the beginning of the healing process [35,36]. Fibrinous/cartilaginous tissue production is observed in the first 3 days, it peaks in about 10 to 12 days, and its removal starts as early as 21 days [33]. Approximately at 28 to 35 days, osteoclasts populate the tissue and the removal of the fibrocartilage is substantially observed [35]. The fracture healing outcome is considered a delayed union if the fibrous/cartilaginous tissue is not removed completely in about 3 to 4 months after the injury, while it is considered a nonunion if no functional bone is obtained in 6 months after the trauma [37].

3. Modeling Assumptions

The most important effects of macrophages on the bone fracture healing process are observed during the inflammatory and repair phases of the bone fracture healing process [17]. During the inflammatory phase, macrophages modulate and resolve the inflammation while during the repair phase macrophages provide an optimal environment for the cellular proliferation, differentiation, and tissue production. The primary cells during the inflammatory and repair phases of the bone fracture healing process are debris (D), unactivated macrophages (M_0), classical macrophages (M_1), alternative macrophages (M_2), MSCs (C_m), and osteoblasts (C_b). It is assumed that the cellular functions are regulated by the tumor necrotic factor-α (c_1) and the interleukin-10 (c_2) cytokines. It is also assumed that the regenerative process is given by the production of two extracellular matrices: the fibrocartilage (m_c), and the woven bone (m_b). These biological system interactions are depicted in Figure 1. The variables represent homogeneous quantities in a given volume.

In Figure 1, the cellular dynamics are represented by the circular shapes and solid arrows. The molecular concentrations and their production/decay are represented by the octagonal shapes and dashed arrows. The pro- and anti-inflammatory cytokines activation/inhibition effects on the cellular functions are represented by the dotted arrows. Removal of debris and the negative effect among the variables are represented by the dot-ending dotted arrows.

It is assumed that unactivated macrophages M_0 do not release cytokines and do not engulf debris. It is also assumed that the population of M_0 increases in size proportionally to the debris concentration up to a maximal value of M_{max} [30]. The only source of activated macrophages, M_1 and M_2, is M_0. Even though both phenotypes of activated macrophages have the abilities to release both pro- and anti-inflammatory cytokines, it is assumed that only M_1 deliver c_1 and M_2 deliver c_2, as those are the major cytokines for each phenotype [38]. M_0 activate to M_1 under the c_1 stimulus, while they activate to M_2 under the c_2 stimulus. M_1 and M_2 macrophages do not de-differentiate back to the M_0 macrophages [39]; and are able to switch phenotypes at a constant rate [32]. The accumulation of macrophages at the injury site is modeled by its recruitment due to inflammation, which is assumed to be proportional to the debris density.

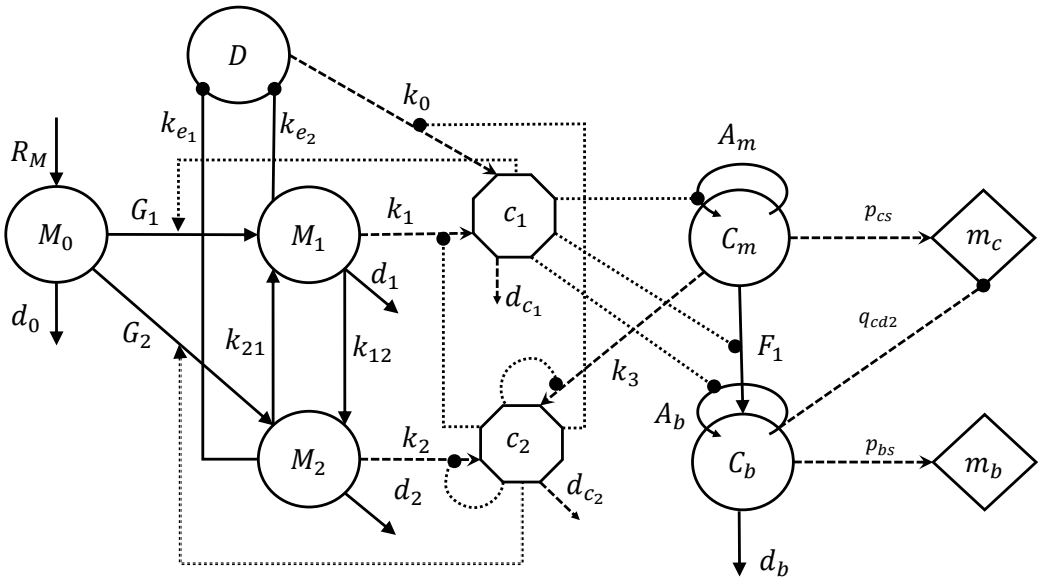

Figure 1. Flow diagram of the cellular and molecular dynamics during the inflammatory and repair phases of the bone fracture healing process.

It is assumed that MSCs differentiate into osteoblasts at a constant rate. MSCs synthesize the fibrocartilage, while osteoblasts synthesize the woven bone. It is also assumed that only the fibrocartilage is constantly removed by the osteoclasts. The density of the osteoclasts is assumed to be proportional to the density of the osteoblasts. The two types of tissue cells increase their populations by proliferation in a logistic growth fashion [33]. It is also assumed that there is no recruitment of MSCs and osteoblasts.

4. Model Formulation

The process of bone fracture healing is modeled with a mass-action system of nonlinear ordinary differential equations. Following the outlined biological assumptions and the flow diagram given in Figure 1 yields the resulting system of equations:

$$\frac{dD}{dt} = -R_D(k_{e_1}M_1 + k_{e_2}M_2) \quad (1)$$

$$\frac{dM_0}{dt} = R_M - G_1M_0 - G_2M_0 - d_0M_0 \quad (2)$$

$$\frac{dM_1}{dt} = G_1M_0 + k_{21}M_2 - k_{12}M_1 - d_1M_1 \quad (3)$$

$$\frac{dM_2}{dt} = G_2M_0 + k_{12}M_1 - k_{21}M_2 - d_2M_2 \quad (4)$$

$$\frac{dc_1}{dt} = H_1(k_0D + k_1M_1) - d_{c_1}c_1 \quad (5)$$

$$\frac{dc_2}{dt} = H_2(k_2M_2 + k_3C_m) - d_{c_2}c_2 \quad (6)$$

$$\frac{dC_m}{dt} = A_mC_m\left(1 - \frac{C_m}{K_{lm}}\right) - F_1C_m \quad (7)$$

$$\frac{dC_b}{dt} = A_bC_b\left(1 - \frac{C_b}{K_{lb}}\right) + F_1C_m - d_bC_b \quad (8)$$

$$\frac{dm_c}{dt} = (p_{cs} - q_{cd1}m_c)C_m - q_{cd2}m_cC_b \quad (9)$$

$$\frac{dm_b}{dt} = (p_{bs} - q_{bd}m_b)C_b \quad (10)$$

Equation (1) describes the rate of change with respect to time of the debris density, which decreases proportionally to M_1 and M_2. The engulfing rate R_D is modeled by a Hill Type II function to represent the saturation of the phagocyte rate of macrophages [38,40]:

$$R_D = \frac{D}{a_{ed} + D}.$$

Equation (2) describes the rate of change with respect to time of the undifferentiated macrophages density. It increases because of migration and decreases by differentiating into M_1 and M_2 or by a constant emigration rate. It is assumed that M_0 migrate to the injury site proportionally to D up to a maximal constant rate, k_{max}, [26,31]:

$$R_M = k_{max}\left(1 - \frac{M}{M_{max}}\right)D,$$

where $M = M_0 + M_1 + M_2$. The differentiation rates of M_0 into M_1 and M_2 are stimulated by the cytokines accordingly to a Hill Type II equations, respectively [32]:

$$G_1 = k_{01} \times \frac{c_1}{a_{01} + c_1}, \quad G_2 = k_{02} \times \frac{c_2}{a_{02} + c_2}.$$

Equation (3) describes the rate of change with respect to time of M_1, which increases when M_0 activate to M_1 and M_2 shift phenotype; and decreases by emigration and when M_1 shift phenotype. Similarly, Equation (4) describes the rate of change with respect to time of M_2. Equations (5) and (6) describes the rate of change with respect to time of c_1 and c_2. Here, k_0, k_1, k_2, and k_3 are the constant rates of the cytokine productions and d_{c_1} and d_{c_2} are the cytokine constant decay rates. The inhibitory effects of the anti-inflammatory cytokines are modeled by the following functions [32]:

$$H_1 = \frac{a_{12}}{a_{12} + c_2}, \quad H_2 = \frac{a_{22}}{a_{22} + c_2}.$$

Equation (7) describes the rate of change with respect to time of C_m, which increases by cellular division up to a constant-maximal carrying capacity, K_{lm}, and decreases by differentiation. The total MSCs proliferation rate is modeled by [28]:

$$A_m = k_{pm} \times \frac{a_{pm}^2 + a_{pm_1} c_1}{a_{pm}^2 + c_1^2},$$

where in the absent of inflammation, $c_1 = 0$, MSCs proliferate at a constant rate k_{pm}. However, when there is inflammation, $c_1 > 0$, the proliferation rate of MSCs increases or decreases according to the concentration of c_1, i.e., high concentration levels of c_1 inhibit C_m proliferation while low concentration levels of c_1 accelerate C_m proliferation. The differentiation rate of C_m is inhibited by c_1, which is modeled by the following function:

$$F_1 = d_m \times \frac{a_{mb_1}}{a_{mb_1} + c_1}.$$

Equation (8) describes the rate of change with respect to time of C_b. It increases when MSCs differentiate into osteoblasts or when osteoblasts proliferate. It decreases at a constant rate d_b when osteoblasts differentiate into osteocytes. The osteoblasts proliferation rate is inhibited by c_1, which is modeled by the following function:

$$A_b = k_{pb} \times \frac{a_{pb}}{a_{pb} + c_1}.$$

Equations (9) and (10) describe the rate of change with respect to time of the fibrocartilage and woven bone, where p_{cs} and p_{bs} are the tissue constant synthesis rates and q_{cd1}, q_{cd2}, and q_{bd} are the tissue degradation rates, respectively [33].

5. Analysis of the Model

The analysis of Model (1)-(10) is done by finding the equilibria and their corresponding stability properties. An equilibrium is a state of the system where the variables do not change over time [41]. Once the equilibria are identified, it is important to determine the behavior of the model near equilibria by analyzing their local stability properties. An equilibrium is locally stable if the system moves toward it when it is near the equilibrium, otherwise it is unstable [41]. Therefore, the equilibria provide the possible outcomes of the bone fracture healing process and their corresponding stability properties define the conditions under which a particular healing result occurs.

System (1)-(10) has the following three biologically meaningful equilibria of the vector form $E = (D, M_0, M_1, M_2, c_1, c_2, C_m, C_b, m_c, m_b)$: $E_0 = (0,0,0,0,0,0,0,0,m_{c_0}^*, m_{b_0}^*)$, $E_1 = (0,0,0,0,0,0,0,K_{lb}(1 - d_b/k_{pb}), 0, p_{bs}/q_{bd})$, $E_2 = (0,0,0,0,0,c_2^*, C_m^*, C_b^*, m_c^*, p_{bs}/q_{bd})$, where $C_m^* = K_{lm}(1 - d_m/k_{pm})$, $C_b^* = K_{lb}(k_{pb} - d_b + \sqrt{(k_{pb} - d_b)^2 + 4k_{pb}d_m C_m^*/K_{lb}})/2k_{pb}$, $c_2^* = a_{22}(-1 + \sqrt{1 + 4k_3 C_m^*/a_{22}d_{c_2}})/2$, and $m_c^* = p_{cs}C_m^*/(q_{cd1}C_m^* + q_{cd2}C_b^*)$. The existence conditions for the three equilibria are summarized in Table 1 and their stability conditions are summarized in Table 2 and proved in Appendix A.

The existence conditions listed in Table 1 arise from the fact that all biologically meaningful variables are nonnegative. Therefore, the existence condition for E_0 requires the steady state tissue densities to be either zero or any positive number. For E_1, the existence condition arises from the requirement that the steady state density of C_b must be greater than zero, which implies that the proliferation rate of osteoblasts must be greater than their differentiation rate, i.e., $k_{pb} > d_b$.

Similarly for E_2, the existence condition arises from the requirement that the steady state density for C_m must be greater than zero, which implies that the proliferation rate of MSCs must be greater than their differentiation rate, i.e., $k_{pm} > d_m$.

Preprints (www.preprints.org) | NOT PEER-REVIEWED | Posted: 16 November 2018 doi:10.20944/preprints201811.0376.v1

Peer-reviewed version available at Math. Comput. Appl. 2019, 24, 12; doi:10.3390/mca24010012

Table 1. Existence conditions for the equilibrium points and their biological meaning.

Equilibrium Points	Existence Conditions	Meaning
$E_0 = (0,0,0,0,0,0,0,0,m^*_{c_0}, m^*_{b_0})$	$m^*_{c_0} \geq 0, m^*_{b_0} \geq 0$	nonunion
$E_1 = (0,0,0,0,0,0,0,K_{lb}(1-d_b/k_{pb}),0,p_{bs}/q_{bd})$	$k_{pb} > d_b$	successful healing
$E_2 = (0,0,0,0,0,c^*_2, C^*_m, C^*_b, m^*_c, p_{bs}/q_{bd})$	$k_{pm} > d_m$	nonunion or delayed union

The stability conditions of each biologically feasible equilibrium are listed in Table 2 and determined from the eigenvalues of its associated Jacobian matrix, see Appendix A, as follows:

E_0 is stable when $k_{pm} \leq d_m$ and $k_{pb} \leq d_b$ (see Theorem A1) which implies that the differentiation rates of the MSCS and osteoblasts are greater than or equal to their proliferation rates, respectively. The steady-state E_0 represents a nonunion. In this case, the inflammation is resolved since the first five entries of E_0 are zero; however, the repair process has failed since the osteoblasts and osteoclasts have died out before the beginning of the remodeling process. Hence, the tissue densities, $m^*_{c_0}$ and $m^*_{b_0}$, can be any two positive values smaller than their maximal densities, p_{cs}/q_{cd1} and p_{bs}/q_{bd}, respectively (see Theorem A1).

E_1 is stable when $k_{pm} \leq d_m$ and $k_{pb} > d_b$ (see Theorem A2). The steady-state E_1 represents a successful repair of the bone fracture, where the inflammation is resolved, the fibrocartilage is completely removed from the repair site, and the woven bone has achieved its maximal density. In this case, osteoblasts proliferate faster than they differentiate while MSCs have the opposite behavior.

E_2 is stable when $k_{pm} > d_m$ (see Theorem A3). The steady-state E_2 represents a nonunion or delayed union, where the inflammation is resolved but the osteoclasts have failed to degrade the cartilage in a timely fashion.

Table 2. Stability conditions for the equilibrium points.

Equilibrium Points	Stability Conditions	Stability
E_0	$k_{pm} \leq d_m, k_{pb} \leq d_b$	E_0 belongs to an attracting local set
E_0, E_1	$k_{pm} \leq d_m, k_{pb} > d_b$	E_0 unstable; E_1 locally stable
E_0, E_2	$k_{pm} > d_m, k_{pb} \leq d_b$	E_0 unstable; E_2 locally stable
E_0, E_1, E_2	$k_{pm} > d_m, k_{pb} > d_b$	E_0 and E_1 unstable; E_2 locally stable

6. Numerical Results

The proposed new model (1)-(10) is used to investigate the evolution of a broken bone under normal and pathological conditions during the first 21 days after trauma. Table 3 summarizes the baseline parameter values and units for the numerical simulations. These values are estimated in a qualitative manner from data in other studies [30,38,39] and are based on murine experiments with healthy mice having a moderate fracture (a broken bone with a gap size less than 3mm) [33,42]. The bone fracture healing process for humans involves the same cells, cytokines, and qualitative dynamics, differing only in the number of cells, concentrations, and the length of time it takes for a full recovery.

First, a set of numerical simulation results is presented to compare two mathematical models of the bone fracture healing process that incorporate macrophages: the model developed in [17] and the new model (1)-(10). Next, numerical simulations are performed to support the theoretical stability results (successful and nonunion equilibria) and to numerically monitor the healing progression of a moderate fracture in normal conditions. Another set of numerical simulations is performed to analyze the effects of different debris densities on bone fracture healing. Finally, a set of numerical simulation results is presented to investigate the effects of different concentrations of anti-inflammatory cytokines and various cellular treatments on the fracture healing under numerous pathological conditions. All simulations are obtained by using the adaptive MATLAB solver `ode23s` and are initiated with densities of debris, macrophages, and MSCs set to $D(0) = 5 \times 10^7$, $M_0(0) = 4000$, $C_m(0) = 1000$, respectively, and the pro-inflammatory cytokines concentration set to $c_1(0) = 1$.

Table 3. Parameter descriptions and units.

Parameter	Description	Range of values	Reference
k_{e_1}	Engulfing debris rate of M_1	$3-48/day$	[38,40]
k_{e_2}	Engulfing debris rate of M_2	$3-48/day$	[38,40]
a_{ed}	Half-saturation of debris	$4.71\times10^6\ cells/mL$	[38]
k_{max}	Maximal migration rate	$0.015-0.1\ /day$	[39,43]
M_{max}	Maximal macrophages density	$6\times10^5-1\times10^6 cells/mL$	[30,40]
k_{01}	Activation rate of M_1	$0.55-0.611\ /day$	[32,39]
k_{02}	Activation rate of M_0 to M_2	$0.0843-0.3\ /day$	[32]
k_{12}	Transition rate from M_1 to M_2	$0.083-0.075\ /day$	[32,39]
k_{21}	Transition rate from M_2 to M_1	$0.005-0.05/\ day$	[32]
d_0	Emigration rate of M_0	$0.156-0.02\ /day$	[32,39]
d_1	Emigration rate of M_1	$0.121-0.2\ /day$	[32,38,39]
d_2	Emigration rate of M_2	$0.163-0.2\ /day$	[32,38,39]
k_0	Secretion rate of c_1 by debris	$5\times10^{-7}-8.5\times10^{-6}\ ng/cells/day$	[38]
k_1	Secretion rate of c_1 by M_1 macrophages	$8.3\times10^{-6}\ ng/cells/day$	[38]
k_2	Secretion rate of c_2 by M_2 macrophages	$3.72\times10^{-6}\ ng/cells/day$	[38]
k_3	Secretion rate of c_2 by MSCs	$7\times10^{-7}-8\times10^{-6}\ ng/cells/day$	[17]
d_{c_1}	Decay rate of c_1	$12.79-55\ /day$	[32,38]
d_{c_2}	Decay rate of c_2	$2.5-4.632\ /day$	[32,38]
a_{12}	Effectiveness of c_2 inhibition of c_1 synthesis	$0.025\ ng/mL$	[32]
a_{22}	Effectiveness of c_2 inhibition of c_2 synthesis	$0.1\ ng/mL$	[32]
a_{pm}	Effectiveness of c_1 inhibition of C_m proliferation	$3.162\ ng/mL$	[17]
a_{mb_1}	Effectiveness of c_1 inhibition of C_b proliferation	$0.1\ ng/mL$	[17]
a_{01}	Half-saturation of c_1 to activate M_1	$0.01\ ng/mL$	[32]
a_{02}	Half-saturation of c_2 to activate M_2	$0.005\ ng/mL$	[32]
a_{pb}	Effectiveness of c_1 inhibition of C_b proliferation	$10\ ng/mL$	[17]
a_{pm_1}	Constant enhancement of c_1 to C_m proliferation	$13\ ng/mL$	[17]
k_{pm}	Proliferation rate of C_m	$0.5\ /day$	[17]
d_m	Differentiation rate of C_m	$1\ /day$	[17]
k_{pb}	Proliferation rate of C_b	$0.2202\ /day$	[17]
d_b	Differentiation rate of C_b	$0.15\ /day$	[17]
p_{cs}	Fibrocartilage synthesis rate	$3\times10^{-6}\ g/cells/day$	[17]
q_{cd_1}	Fibrocartilage degradation rate	$3\times10^{-6}\ mL/cells/day$	[17]
q_{cd_2}	Fibrocartilage degradation rate by osteoclasts	$0.2\times10^{-6}\ mL/cells/day$	[17]
p_{bs}	Bone tissue synthesis rate	$5\times10^{-8}\ g/cells/day$	[17]
q_{bd}	Bone tissue degradation rate	$5\times10^{-8}\ mL/cells/day$	[17]
K_{lb}	Carrying capacity of C_b	$1\times10^6\ cells/mL$	[17]
K_{lm}	Carrying capacity of C_m	$1\times10^6\ cells/mL$	[17]
$D(0)$	Density of necrotic cells	$1\times10^6-2\times10^8\ cells/mL$	[30,38,40]
$C_m(0)$	Initial MSCs density	$1000\ cells/mL$	[17]
$M_0(0)$	Unactivated macrophage density	$4000\ cell/mL$	[43]

6.1. Comparison of existing models

The model developed in [17] and the present mathematical model (1)-(10) are compared when $D(0) < a_{ed} = 4.71\times10^6$, i.e., the initial debris concentration is below the half-saturation of debris. In this case, the macrophages' digestion rate increases approximately linearly with respect to the debris population, as it is assumed in model [17]. The same parameter values are used in both models (Table 3), with $k_{e_1} = 11$, $k_{e_2} = 48$, $k_2 = 3.72\times10^{-6}$, and $k_3 = 8\times10^{-6}$.

Figure 2 shows the numerical evolutions of the tissues' production when $D(0) = 2\times10^6$. In all simulations, we refer to fibrocartilage and woven bone as cartilage and bone, respectively. The production of cartilage m_c and bone m_b given by the present model is much more realistic than the production given by the model developed [17], since, according to the experimental data, the cartilage production peaks to its maximal density of around $1g/mL$ about 10-12 days after trauma and a significant bone tissue production is observed after the second week [44].

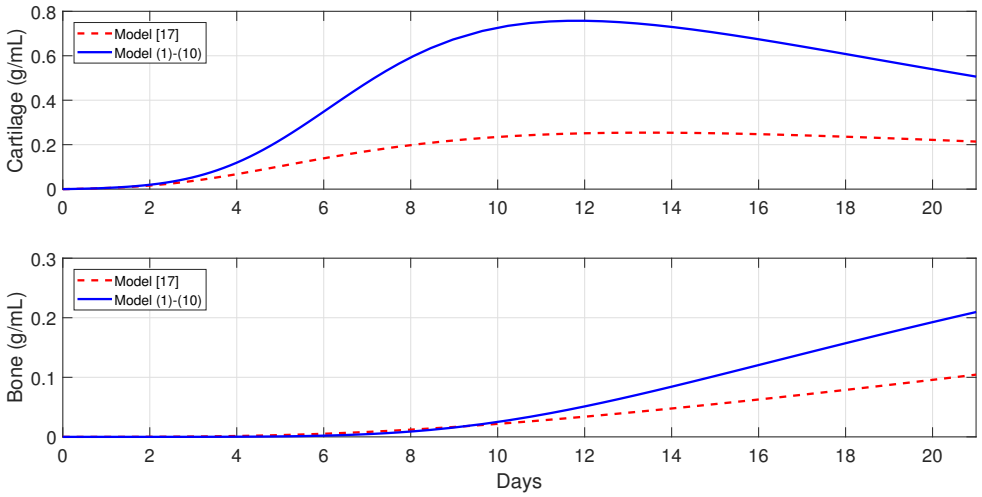

Figure 2. Comparison of tissues evolution in Model [17] and Model (1)-(10).

6.2. *Different outcomes of the bone fracture healing process*

Next, a set of numerical simulations is presented to support the theoretical results. Accordingly to the qualitative analysis of the model there are three equilibria: E_0, E_1 and E_2 where their stability conditions are determined by the tissue cells' proliferation and differentiation rates, k_{pm}, k_{pb}, d_m and d_b, respectively. The following parameter values are used: $k_{pm} = 0.5$, $d_m = 1$, $k_{pb} = 0.2202$, and $d_b = 0.3$, to demonstrate the stability of E_0, since then $k_{pm} < d_m$ and $k_{pb} < d_b$. The stability of E_1 is demonstrated using the following parameter values: $d_m = 1$, $k_{pm} = 0.5$, $k_{pb} = 0.2202$, and $d_b = 0.15$, since then $k_{pm} \leq d_m$ and $k_{pb} > d_b$. Finally, the following parameter values are used: $k_{pm} = 0.5$ and $d_m = 0.1$, to demonstrate the stability of E_2, since then $k_{pm} > d_m$. Different time-periods are used in Figures 3-5 to better demonstrate the qualitative behavior of the system under different stability conditions.

Figure 3 shows the qualitative behavior of E_1 for the macrophages, debris, TNF-α, and IL-10 densities, with the inflammation being resolved in about 40 days. The top-left plot of Figure 3 shows the temporal evolution of M_0 (dashed lines), M_1 (dotted lines), and M_2 (solid lines). It can be observed that M_1 first peaks to its maximum value, which is then followed by M_2. Similar sequences of transitions of first M_1 and then M_2 are commonly observed in normal tissue healing conditions [5,39].

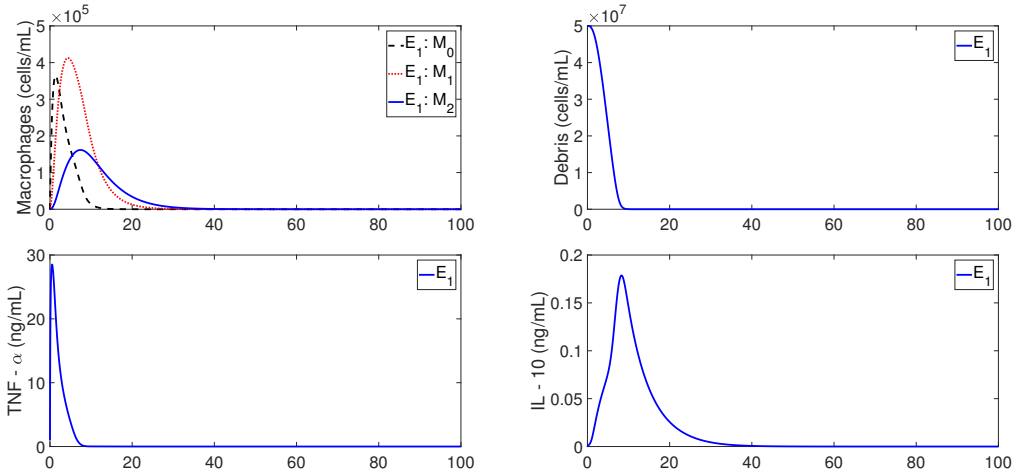

Figure 3. Cellular and molecular evolution of the resolution of the inflammation in normal conditions.

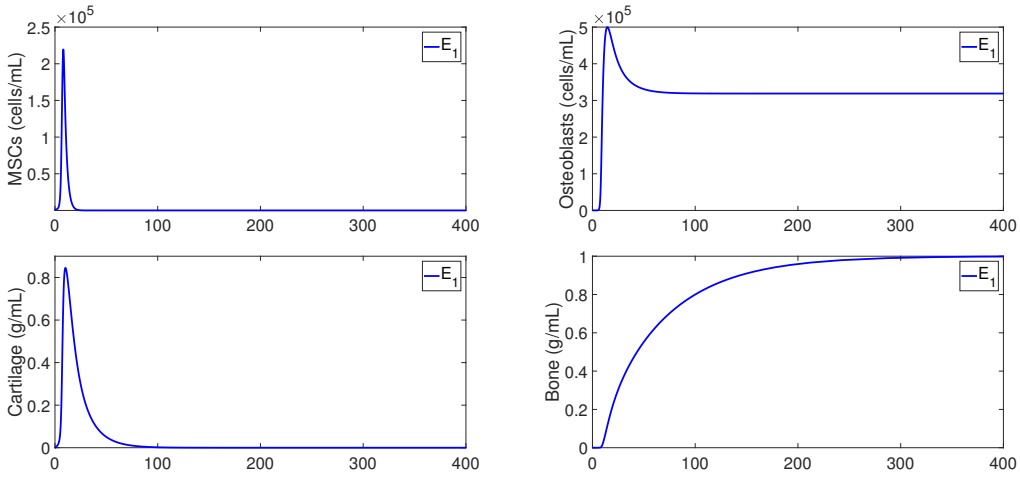

Figure 4. Cellular and molecular evolution of the repair process in a successful fracture healing.

Figure 4 shows the qualitative behaviors of E_1 for the MSCs, osteoblasts, cartilage, and bone densities. Here, the MSCs density decays to zero over the time, while the osteoblasts maintain a constant density below their carrying capacity $K_{lb} = 1 \times 10^6$. In addition, the bottom plots of Figure 4 show that the cartilage is eventually degraded by the osteoclasts and the bone achieves its maximum density of 1 ng/mL. Therefore, E_1 exhibits the temporal progression of a successful bone fracture healing.

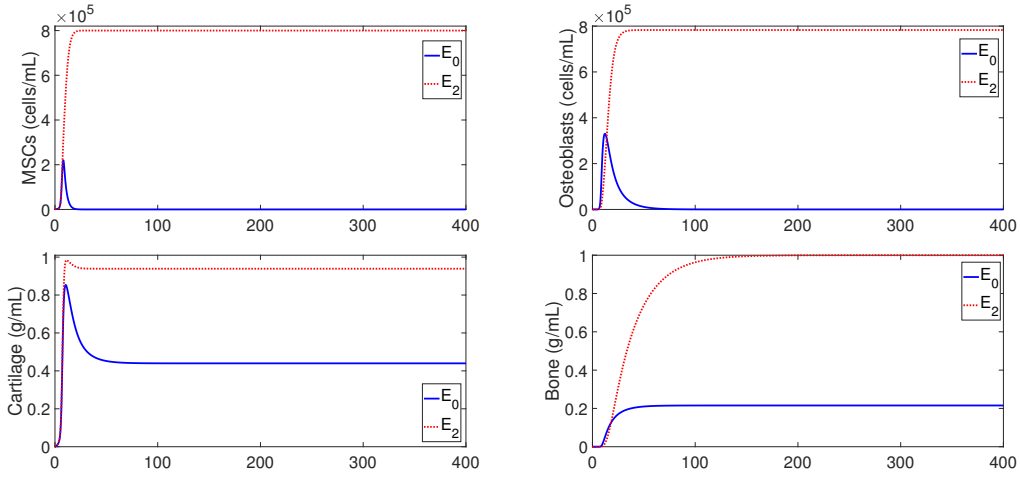

Figure 5. Cellular and molecular evolution of the repair process in a nonunion fracture healing.

Figure 5 shows the qualitative evolution for the MSCs, osteoblasts, cartilage, and bone densities for E_0 (solid lines) and E_2 (dotted lines). Since the temporal evolution of macrophages, debris, and cytokines densities in E_0 and E_2 are similar to those for E_1 showed in Figure 3, then they are omitted here. It can be observed in Figure 5 that the two cellular densities in E_0, MSCs and osteoblasts, decay to zero over the time, with the osteoclasts failing to degrade the cartilage; which results in nonunion. Mathematically, this case occurs when osteoblasts proliferate at a rate lower than their differentiation rate, i.e., $k_{pb} < d_b$. In practice, this scenario is commonly observed in advanced-age patients whose MSCs and osteoblast cells decrease their capability to proliferate and differentiate [1]. On the other hand, the two cells and the two tissues in E_2 remain at positive constant values (Figure 5), but the final fracture healing outcome is still a nonunion. Here, the osteoclasts again fail to degrade the cartilage [1], even though the bone has achieved its maximum density of 1 ng/mL. Therefore, in this case, migration

Peer-reviewed version available at Math. Comput. Appl. 2019, 24, 12; doi:10.3390/mca24010012

of osteoclasts must be enhanced through surgical interventions in order to achieve a successful bone repair [33].

6.3. Evolution of the healing process for different types of fractures

In this section, the model is used to monitor the evolution of a successful repair (Table 3) for different types of fractures. In healthy individuals, the simple, moderate, and severe fractures are correlated with the debris densities [45,46]. Therefore, the initial debris concentration is set to $D(0) = 3 \times 10^5$, $D(0) = 5 \times 10^7$, and $D(0) = 2 \times 10^8$, for a simple, moderate, and severe fracture, respectively.

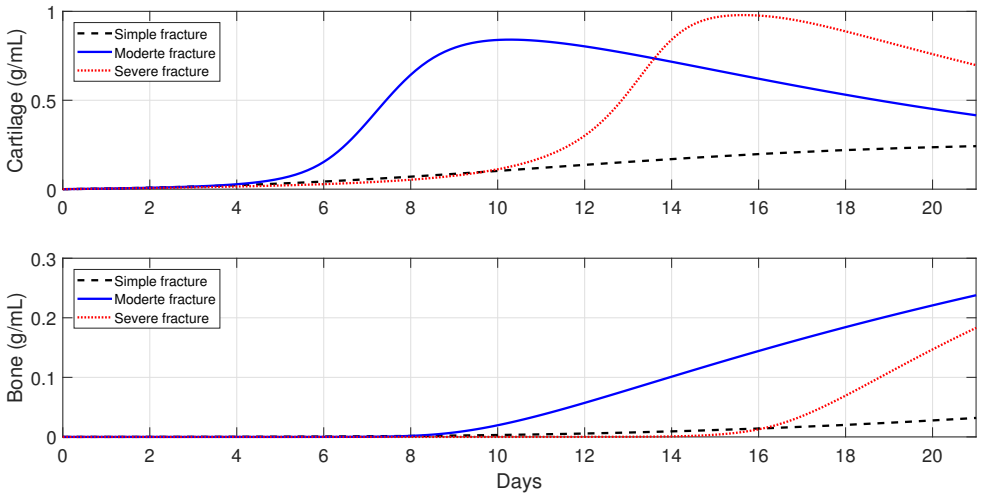

Figure 6. Tissues evolution of a successful repair for different types of fractures.

Figure 6 shows that the tissues production is a slow process for a simple fracture, since the cartilage and bone densities are less than the corresponding tissue densities for moderate and severe fractures. Slow healing process is commonly observed in micro-crack healing [45]. Furthermore, there is less cartilage formation over time in simple fractures [46]. For a moderate fracture, the maximal production of the cartilage is observed around 10 days followed by a significant degradation, while the bone tissue production occurs after the first week. For a severe fracture, Figure 6 shows that there is a delay in the two tissues production compared with those given by moderate fractures, with the peak of the cartilage and bone productions observed at around day 16.

6.4. Immune-modulation therapeutic treatments to accelerate bone fracture healing

The administration of anti-inflammatory drugs and the injection and/or transplantation of MSCs and macrophages are two of the clinical trials that have been implemented in orthopedics to stimulate and accelerate bone fracture healing [5,15]. In this section, Model (1)-(10) is used to explore these possible therapeutic treatments to accelerate the healing of a broken bone under normal and pathological conditions such as severe fractures, advanced age, and senil osteoporosis [1].

6.4.1. Administration of anti-inflammatory drugs at the beginning of the healing process

A set of numerical simulations is presented to investigate the effect of the administrations of anti-inflammatory cytokines at the beginning of the healing process in healthy individuals and also in immune-compromised patients. In each case of the numerical simulations, $c_2(0) = 0$, 10 and 100 ng/mL.

In healthy individuals, the administration of anti-inflammatory drugs is implemented for a simple fracture and also for two moderate fractures with different debris concentrations: $D(0) = 3 \times 10^5$, $D(0) = 2 \times 10^7$, and $D(0) = 5 \times 10^7$.

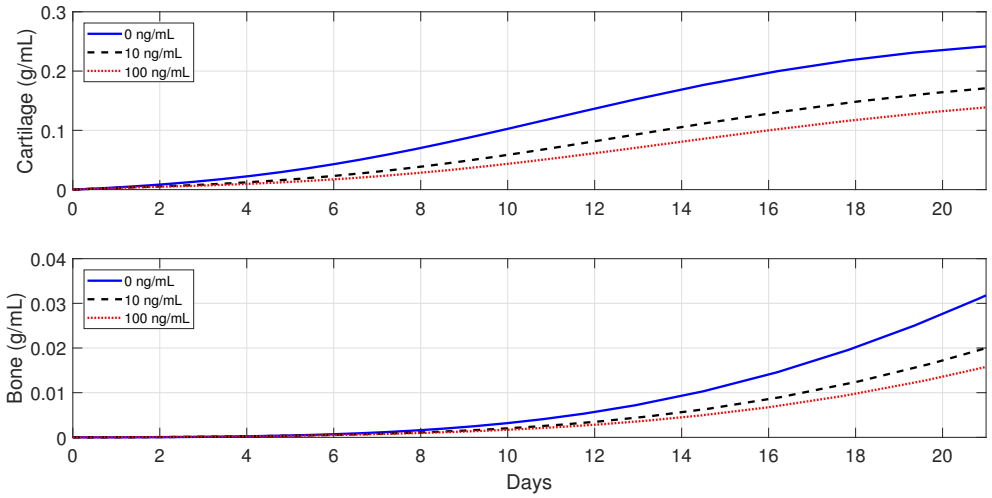

Figure 7. Tissues evolution in a simple fracture under different initial anti-inflammatory cytokines concentrations, $D(0) = 3 \times 10^5$.

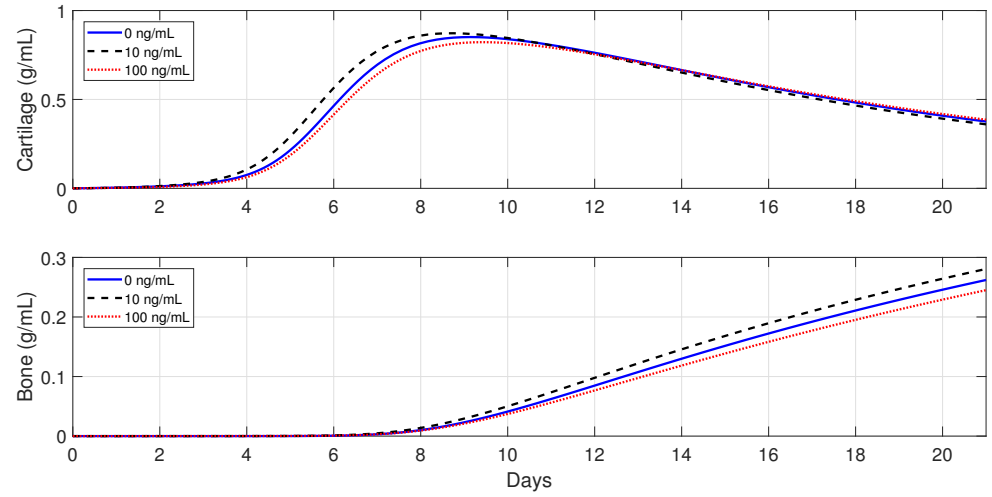

Figure 8. Tissues evolution in a moderate fracture under different initial anti-inflammatory cytokines concentrations, $D(0) = 2 \times 10^7$.

Figure 7 shows that the administration of c_2 in the simple fracture slows down both the cartilage and bone productions. Figures 8 and 9 show that the administration of c_2 in the moderate fractures improves the tissues evolution but in a dose-dependent manner. On one hand, when $D(0) = 2 \times 10^7$ the administration of c_2 has either a positive or negative effect on the two tissue productions. The administration of 10 ng/mL of c_2 enhances the early production of cartilage and increases the bone synthesis, while the administration of 100 ng/mL of c_2 results in the opposite effect. On the other hand, when $D(0) = 5 \times 10^7$ the administration of c_2 enhances the earlier cartilage production and improves the synthesis of the bone for both concentrations, with 10 ng/mL being the optimal of the two doses.

Preprints (www.preprints.org) | NOT PEER-REVIEWED | Posted: 16 November 2018 doi:10.20944/preprints201811.0376.v1

Peer-reviewed version available at Math. Comput. Appl. 2019, 24, 12; doi:10.3390/mca24010012

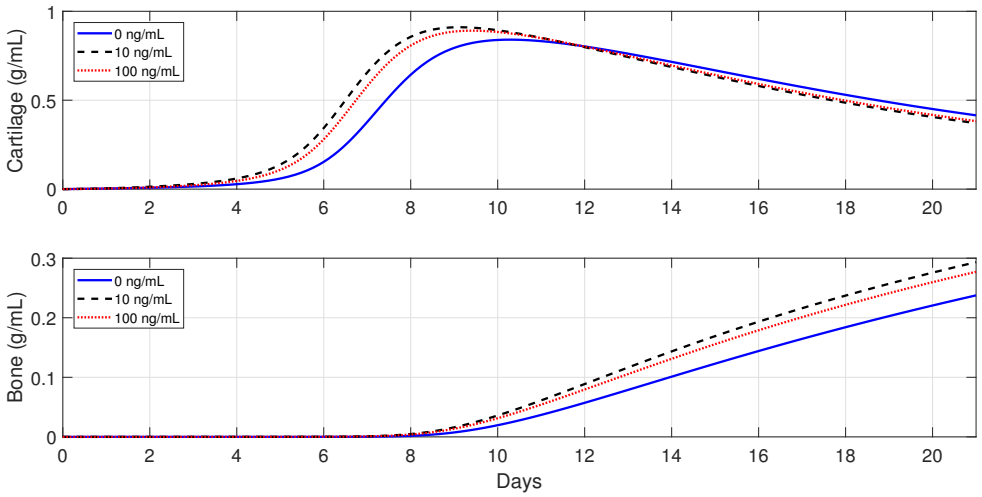

Figure 9. Tissues evolution in a moderate fracture under different initial anti-inflammatory cytokines concentrations, $D(0) = 5 \times 10^7$.

Next, the model is used to implement the administration of anti-inflammatory drugs under different pathological conditions. First, severe fractures in immune-compromised individuals are simulated by using the following parameter values: $D(0) = 2 \times 10^8$ and $k_{max} = 0.0015$, since in fractures of such individuals there is an increase in the accumulation of debris [46] and a decrease in the macrophages migration rate [47]. Second, the following parameter values are used: $k_{e_1} = k_{e_2} = 3$ and $k_1 = 9 \times 10^{-6}$ to simulate bone fracture healing in aging individuals, since in this case, the macrophages phagocytic rate decreases and there is an increase of pro-inflammatory cytokine synthesis by M_1 [1,48]. Finally, $c_1(0) = 100$, $k_{pm} = 0.2$, $d_m = 0.5$, $k_{pb} = 0.16$, and $d_b = 0.15$ are used to simulate the healing process for an senil osteoporotic fracture, since in this case a high level of pro-inflammatory cytokines is observed and the MSCs and osteoblast functions decrease [1].

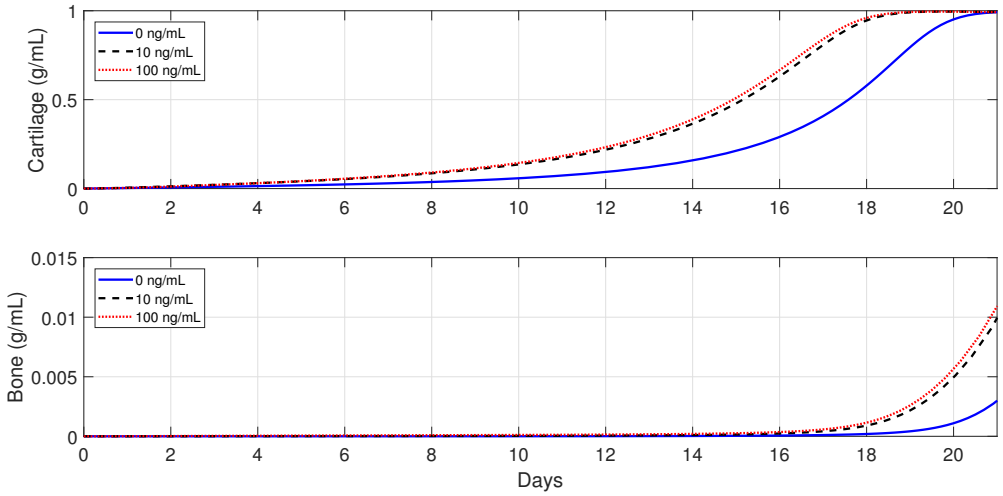

Figure 10. Tissues evolution in a severe fracture under different initial anti-inflammatory cytokines concentrations.

Peer-reviewed version available at Math. Comput. Appl. 2019, 24, 12; doi:10.3390/mca24010012

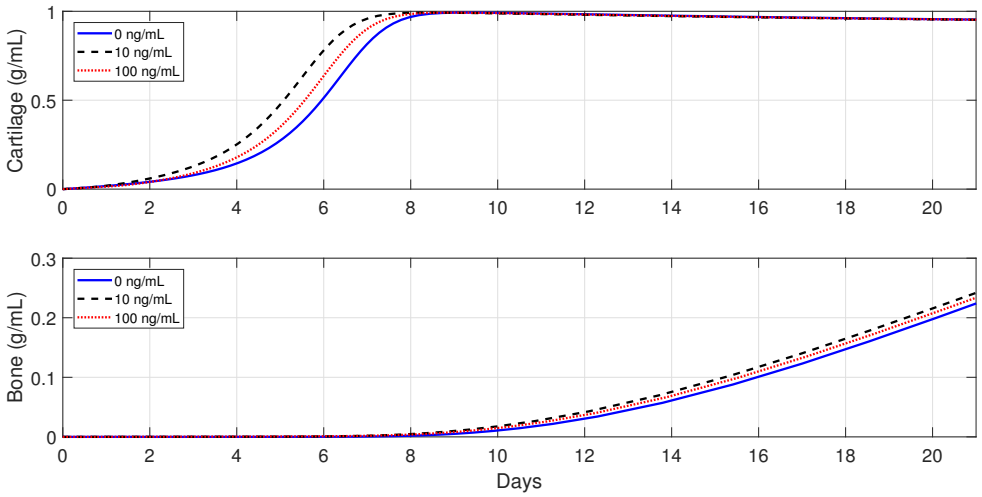

Figure 11. Tissues evolution in an advanced age fracture under different initial anti-inflammatory cytokines concentrations.

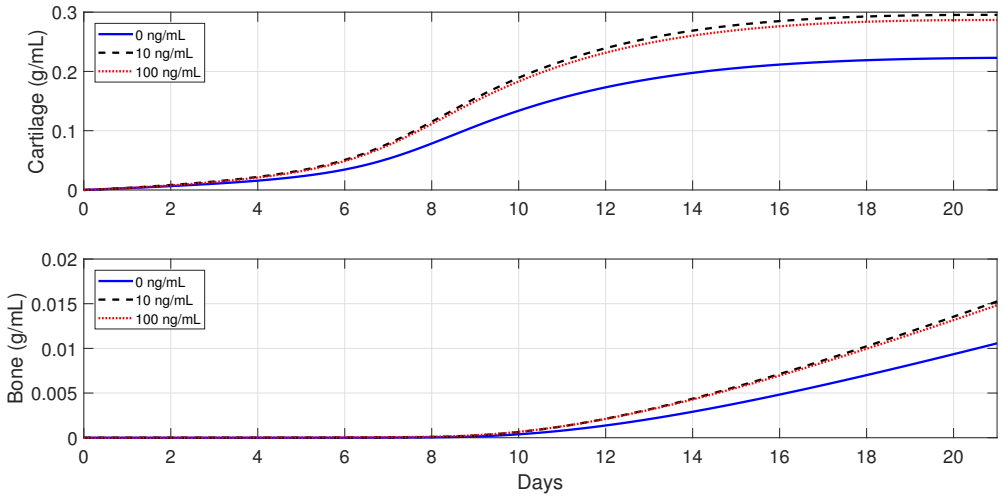

Figure 12. Tissues evolution in a senil osteoporotic fracture under different initial anti-inflammatory cytokines concentrations.

Figures 10, 11, and 12 show that the administration of anti-inflammatory cytokines under the above three under different pathological conditions always improve tissues productions; where the optimal dose of c_2 for both the advanced-age individuals and senil osteoporotic fractures is 10 ng/mL.

6.4.2. Cellular therapeutic interventions under immune-compromised conditions

Additions of MSCs to the injury site through injection and/or transplantation have been used in practice to stimulate and augment bone fracture healing [5]. Another cellular intervention is the scaffold implants, where undifferentiated macrophages and MSCs are co-cultured together, and cytokines are slowly released to stimulate M_2 activation [1]. The parameter values used in the numerical simulations that explore these possible therapeutic treatments are the same as in Subsection 6.4.1.

For severe fractures with immune-compromised conditions, the use of scaffold implants is simulated through a fast M_2 activation, i.e., $k_{02} = 0.3$ and $k_{12} = 0.075$, and also an increase in the

Peer-reviewed version available at Math. Comput. Appl. 2019, 24, 12; doi:10.3390/mca24010012

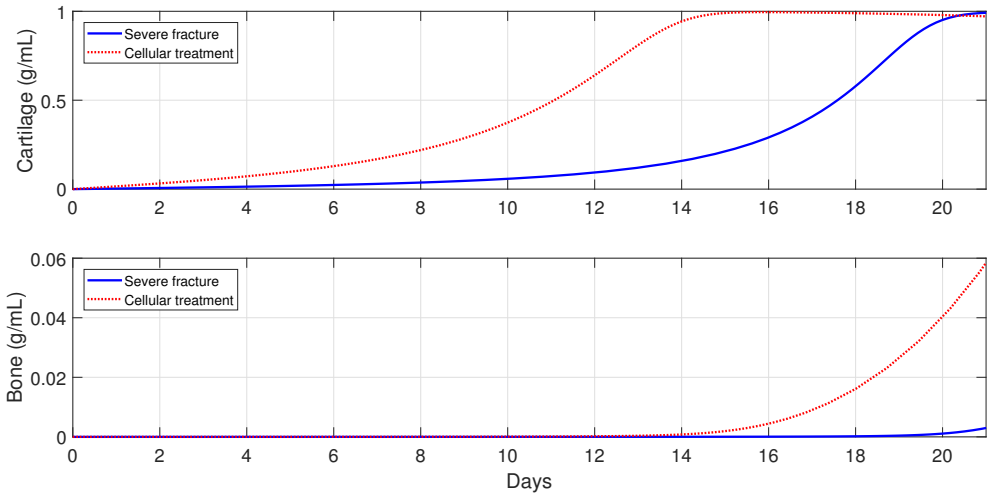

Figure 13. Tissues evolution in a severe fracture without therapeutic innervation (solid line) and with $M_0(0)$ and $C_m(0)$ transplantation (dotted line).

C_m and M_0 densities, i.e., $M_0(0) = 5000$ and $C_m(0) = 5000$. For fractures in aging individuals and individuals with senil osteoporotic fractures, the MSCs injection and the fast M_2 activation are simulated by setting $C_m(0) = 5000$ and $k_{02} = 0.3$ and $k_{12} = 0.075$.

Figures 13, 14, and 15 show that the two cellular interventions increase both tissues productions. Furthermore, those interventions result in larger improvements in severe and senil osteoporotic fractures when compared to fractures in aging individuals.

7. Discussion and Conclusions

A new mathematical model was introduced to mathematically and numerically study the complexity of the molecular and cellular interactions during the bone fracture healing process. The model examined the macrophages functions and their interactions with the tissue cells during the inflammation and repair phases of the healing process. Classically and alternatively activated macrophages were incorporated to mathematically represent their capabilities to modulate and resolve the inflammation. It also included the macrophages abilities to regulate the tissue cellular functions by the delivery of pro- and anti-inflammatory cytokines. In the new model, the resolution of the inflammation is initiated with the activation of the macrophages into their classical phenotype. The classically activated macrophages deliver the pro-inflammatory cytokine TNF-α as they engulf debris. Then the alternatively activated macrophages and the MSCs modulate the inflammation by releasing the anti-inflammatory cytokine IL-10. Finally, the classically activated macrophages remove the remaining debris. The model also incorporated the different engulfing rates of activated macrophages, the saturation rates of phagocytes, and the maximal density of macrophages at the injury site thus allowing a better understanding of the interplay between macrophages and tissue cells during the bone fracture healing process.

The mathematical analysis revealed that there are three feasible fracture healing outcomes. Two of the outcomes represent a nonunion healing: one is the case when the cells deactivate or die out before the healing process finishes up and the other is the case when the tissue cells remain constant but the osteoclasts fail to completely remove the cartilage. The third outcome represents a successful healing, where the osteoblasts and osteoclasts are constantly producing and removing the woven bone. The stability conditions of each outcome can be used to biologically explain why the fracture healing fails as well as to design therapeutic interventions to stimulate or accelerate the healing process.

Peer-reviewed version available at Math. Comput. Appl. 2019, 24, 12; doi:10.3390/mca24010012

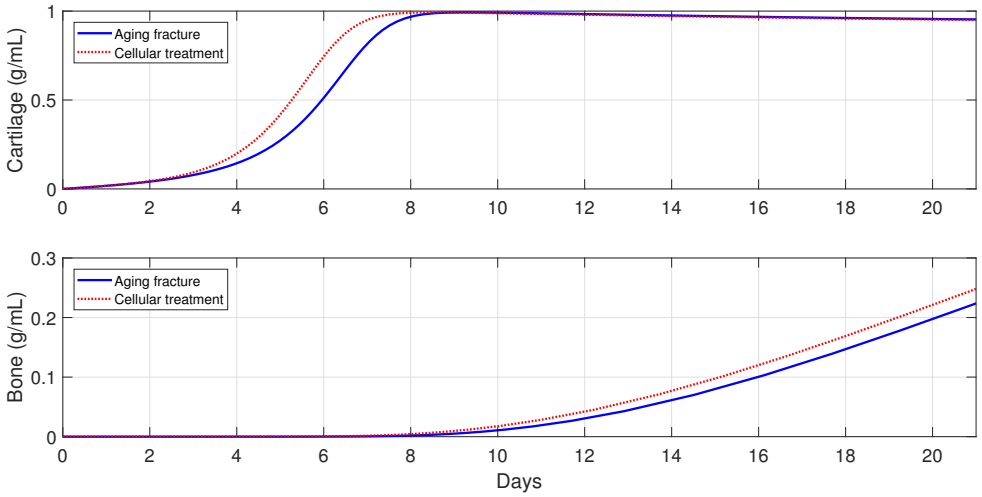

Figure 14. Tissues evolution in an aging fracture without therapeutic innervation (solid line) and with MSCs injection (dotted line).

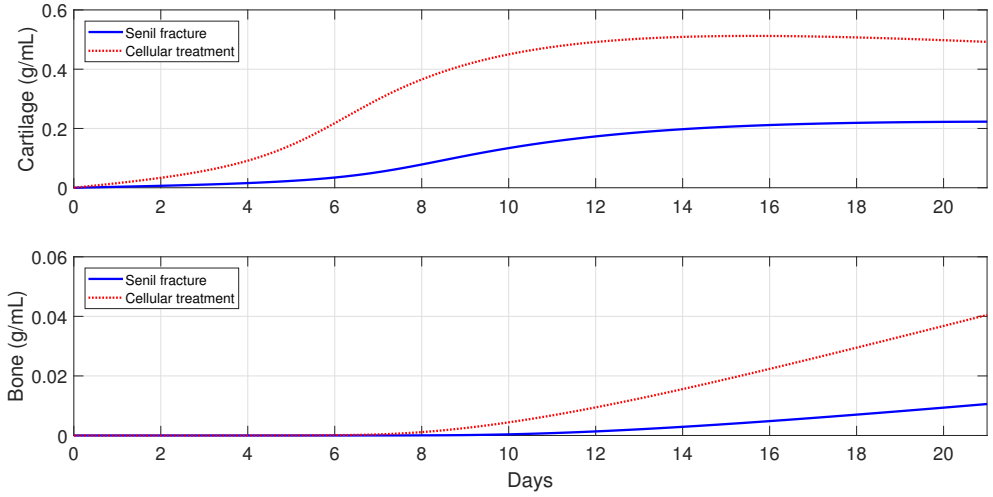

Figure 15. Tissues evolution in a senil osteoporotic fracture without therapeutic innervation (solid line) and with MSCs injection (dotted line).

The new mathematical model allowed a variety of different types of numerical simulations to be performed quickly and cost effectively. It was used to monitor the progression of the healing of a broken bone as well as to predict the final outcome of the healing process. In particular, it was used to numerically simulate the administration of anti-inflammatory drugs to improve the bone fracture healing process. It was found that the administration of anti-inflammatory cytokines fails to accelerate the healing process in simple fractures, while it accelerates the healing process in moderate fractures depending on the cytokine concentrations, and always improves the healing process in severe fractures. Such results have been also clinically observed when corticosteroids and nonsteroidal anti-inflammatory drugs (NSAIDs) are administered in bone fractures [15]. Therefore, based on the model findings, the concentration of debris must be carefully considered when administering anti-inflammatory drugs to enhance the fracture healing process [46]. The model was also used to explore other potential cellular therapeutic approaches, such as the MSCs injection and transplantation. It was found that such treatments can also improve the healing time of a broken bone, especially in immune-compromised patients. The model can also be easily adapted to other therapeutic approaches, such as the administration of different anti-inflammatory drugs, suggesting a variety of possible ways to guide clinical experiments and bone tissue engineering strategies.

Acknowledgments: The first author, IT, was supported by the Mexico's CONACyT and the University of Texas at Arlington.

Author Contributions: All authors contributed equally to the work reported.

Conflicts of Interest: The authors declare no conflict of interest. The founding sponsors had no role in the design of the study; in the collection, analyses, or interpretation of data; in the writing of the manuscript, and in the decision to publish the results.

Appendix

The stability conditions of the equilibria of Model (1)-(10) are stated and proved below. The analysis is conducted using the Jacobian of the system at each equilibrium point and finding its corresponding eigenvalues [41,49].

Theorem A1. *The* $E_0 = \{(0,0,0,0,0,0,0,0,m^*_{c_0}, m^*_{b_0})$ *belongs to the set* $B = \{(0,0,0,0,0,0,0,0,m_c, m_b) : 0 \leq m_c \leq p_{cs}/q_{cd_1}, 0 \leq m_b \leq p_{bs}/q_{bd}\}$, *which is a local attractor set of the solution set given by System (1)-(10) if and only if* $k_{pm} \leq d_m$ *and* $k_{pb} \leq b_d$.

Proof of Theorem A1. The right-hand side functions of System (1)-(10) are continuous and bounded, since all model variables and parameters are positive. Hence, for each initial condition of the system, there is a unique solution [49]. Then, as zero is a solution of the System (1)-(10) and by uniqueness of solution, all the solutions of the system with positive initial condition are positive [49].

Next, it will be proved that the hyperplane $A = \{(0,0,0,0,0,0,0,0,m_c, m_b) : m_c \geq 0, m_b \geq 0\}$ is an attractor set of the solutions of the system (1)-(10). There are two cases to consider based on the relation between the cells proliferation and differentiation rates.

First, let us examine the case when $k_{pm} < d_m$ and $k_{pm} < d_b$. The Jacobian matrix $J(E_0)$ is given by the following lower triangular block matrix

$$J(E_0) = \begin{pmatrix} J_1(E_0) & \mathbf{0} & \mathbf{0} \\ * & J_2(E_0) & \mathbf{0} \\ \mathbf{0} & * & J_3(E_0) \end{pmatrix},$$

where

$$J_1(E_0) = \begin{pmatrix} 0 & 0 & 0 & 0 \\ k_{max} & -d_0 & 0 & 0 \\ 0 & 0 & J_{11} & 0 \\ k_0 & 0 & * & -d_{c_1} \end{pmatrix}, \quad J_2(E_0) = \begin{pmatrix} -d_{c_2} & k_3 & 0 \\ 0 & -d_m + k_{pm} & 0 \\ 0 & d_m & -d_b + k_{pb} \end{pmatrix}$$

$$J_{11} = \begin{pmatrix} -d_1 - k_{12} & k_{21} \\ k_{12} & -d_2 - k_{21} \end{pmatrix}, \quad J_3(E_0) = \begin{pmatrix} 0 & 0 \\ 0 & 0 \end{pmatrix}.$$

Therefore the corresponding characteristic polynomial associated with $J(E_1)$ is given by the product of the characteristic polynomials associated with each submatrix [50]:

$$p(\lambda) = \lambda^3 (\lambda + d_0)(\lambda + d_{c_1})(\lambda + d_{c_2})(\lambda + d_m - k_{pm})(\lambda + d_b - k_{pm})(\lambda^2 + a\lambda + b),$$

where $a = d_1 + d_2 + k_{12} + k_{21}$ and $b = k_{12}d_2 + k_{21}d_1 + d_1d_2$. The polynomial factor of order two of $p(\lambda)$ has the following two roots: $(-a \pm \sqrt{a^2 - 4b})/2$, which are negative since $a^2 - 4b = (d_1 - d_2 + k_{12} - k_{21})^2 + 4k_{12}k_{21} > 0$ and $b > 0$. Therefore, the eigenvalues of $J(E_0)$ are negative for the variables M_0, M_1, M_2, c_1, c_2, C_m, and $C_b$and are equal to zero for D, m_c, and m_b. Since $D'(t) \leq 0$ for all the variables in the system (1)-(10) and $(D^*, 0, 0, 0, 0, 0, 0, 0, m_c, m_b)$ with $D^* \neq 0$ is not an equilibrium point, then the solutions of the system (1)-(8) are attracted to the set $A = \{(0, 0, 0, 0, 0, 0, 0, 0, m_c, m_b) : m_c \geq 0, m_b \geq 0\}$. Equations (9) and (10) imply that $m_c' \leq 0$ and $m_b' \leq 0$ for all $m_c > p_{cs}/q_{cd_1}$ and $m_b > p_{bs}/q_{bd}$. Therefore, the set B is a local attractor set of A [49].

Next, let us consider the case when $k_{pm} = d_m$ and $d_b = k_{pb}$. Here, the eigenvalues of $J(E_0)$ are the same as above except those associated with C_m and C_b, which are equal to zero. Therefore, in this case, by considering the second order approximations of the right hand sides of Equations (7) and (8), instead of just the first order approximations, and using similar arguments as above, proves that the set B is a local attractor set of A. □

Theorem A2. *The equilibrium $E_1 = (0, 0, 0, 0, 0, 0, 0, K_{lb}(1 - d_b/k_{pb}), 0, p_{bs}/q_{bd})$ is locally stable if and only if $d_m \geq k_{pm}$ and $k_{pb} > d_b$.*

Proof of Theorem A2. The Jacobian matrix corresponding to the point E_1 is given by the following lower triangular block matrix

$$J(E_1) = \begin{pmatrix} J_1(E_1) & \mathbf{0} & \mathbf{0} \\ * & J_2(E_1) & \mathbf{0} \\ \mathbf{0} & * & J_3(E_1) \end{pmatrix},$$

where $J_2(E_1)$ has the same expression as $J_1(E_0)$ defined in Theorem A1 and

$$J_2(E_1) = \begin{pmatrix} -d_{c_2} & k_3 & 0 \\ 0 & -d_m + k_{pm} & 0 \\ 0 & d_m & d_b - k_{pb} \end{pmatrix}, \quad J_3(E_1) = \begin{pmatrix} -q_{cd_2}K_{lb}(1 - \frac{d_b}{k_{pb}}) & 0 \\ 0 & -q_{bd}K_{lb}(1 - \frac{d_b}{k_{pb}}) \end{pmatrix}.$$

Since $d_m - k_{pm} \geq 0$ and $k_{pb} > d_b$ and all the eigenvalues of $J_1(E_0)$ are non-positive values, then the eigenvalues of $J(E_1)$ are negative except the eigenvalues associated with D and C_m when $k_{pm} = d_m$, which are equal to zero. Therefore, E_1 is a locally stable node, since $D' \leq 0$ for all the variables of the system (1)-(10) and $C_m' \leq 0$ when $k_{pm} = d_m$. □

Theorem A3. *The equilibrium* $E_2 = (0,0,0,0,c_2^*, C_m^*, C_b^*, m_c^*, p_{bs}/q_{bd})$ *is locally stable if and only if* $k_{pm} > d_m$, *where* $C_m^* = K_{lm}(1 - d_m/k_{pm})$, $C_b^* = K_{lb}(k_{pb} - d_b + \sqrt{(k_{pb} - d_b)^2 + 4k_{pb}d_m C_m^*/K_{lb}})/2k_{pb}$, $c_2^* = a_{22}(-1 + \sqrt{1 + 4k_3 C_m^*/a_{22}d_{c_2}})/2$, *and* $m_c^* = p_{cs}C_m^*/(q_{cd1}C_m^* + q_{cd2}C_b^*)$.

Proof of Theorem A3. The Jacobian matrix corresponding to the point E_2 is given by the following lower triangular block matrix

$$J(E_2) = \begin{pmatrix} J_1(E_2) & \mathbf{0} & \mathbf{0} \\ * & J_2(E_2) & \mathbf{0} \\ \mathbf{0} & * & J_3(E_2) \end{pmatrix},$$

where

$$J_1(E_2) = \begin{pmatrix} 0 & 0 & 0 & 0 \\ k_{max} & -d_0 - G_2^* & 0 & 0 \\ 0 & * & J_{11} & 0 \\ k_0 H_1^* & 0 & * & -d_{c_1} \end{pmatrix}, \quad J_3(E_2) = \begin{pmatrix} -q_{cd_1}C_m^* - q_{cd_2}C_b^* & 0 \\ 0 & -q_{bd}C_b^* \end{pmatrix},$$

$$J_2(E_2) = \begin{pmatrix} -d_{c_2}\left(1 + \frac{c_2^*}{a_{22}+c_2^*}\right) & k_3 H_2^* & 0 \\ 0 & d_m - k_{mb} & 0 \\ 0 & d_m & -\sqrt{(d_b - k_{pb})^2 + 4\frac{k_{bp}d_m C_m^*}{K_{lb}}} \end{pmatrix},$$

$G_2^* = \frac{c_2^* k_{02}}{a_{02}+c_2^*}$, $H_1^* = \frac{a_{12}}{a_{12}+c_2^*}$, $H_2^* = \frac{a_{22}}{a_{22}+c_2^*}$ and J_{11} is defined as in Theorem A1. Since all the eigenvalues of J_{11} are negative (Theorem A1) and $k_{pm} > d_m$, and all equilibrium variables and parameter values are positive, then all the eigenvalues of $J_1(E_2)$, $J_2(E_2)$, $J_3(E_2)$ are negative except for the eigenvalue associated to D which is equal to zero. Therefore, since $D' \leq 0$ for all the variable system, then E_2 is locally stable. □

1. Loi, F.; Córdova, L.A.; Pajarinen, J.; Lin, T.h.; Yao, Z.; Goodman, S.B. Inflammation, fracture and bone repair. *Bone* **2016**, *86*, 119–130.
2. Pisani, P.; Renna, M.D.; Conversano, F.; Casciaro, E.; Di Paola, M.; Quarta, E.; Muratore, M.; Casciaro, S. Major osteoporotic fragility fractures: Risk factor updates and societal impact. *World journal of orthopedics* **2016**, *7*, 171.
3. Teng, G.G.; others. Mortality and osteoporotic fractures: is the link causal, and is it modifiable? *Clinical and experimental rheumatology* **2008**, *26*, S125.
4. Schmidt-Bleek, K.; Kwee, B.J.; Mooney, D.J.; Duda, G.N. Boon and bane of inflammation in bone tissue regeneration and its link with angiogenesis. *Tissue Engineering Part B: Reviews* **2015**, *21*, 354–364.
5. Kovach, T.K.; Dighe, A.S.; Lobo, P.I.; Cui, Q. Interactions between MSCs and immune cells: implications for bone healing. *Journal of immunology research* **2015**, *2015*.
6. Foundation, I.O. Osteoporosis facts and statistics. Data and publication, International Osteoporosis Foundation, 2017.
7. Carlier, A.; Geris, L.; Lammens, J.; Van Oosterwyck, H. Bringing computational models of bone regeneration to the clinic. *Wiley Interdisciplinary Reviews: Systems Biology and Medicine* **2015**, *7*, 183–194.
8. Huber-Lang, M.; Kovtun, A.; Ignatius, A. The role of complement in trauma and fracture healing. Seminars in immunology. Elsevier, 2013, Vol. 25, pp. 73–78.
9. Zhou, Z.; Redaelli, A.; Johnell, O.; Willke, R.J.; Massimini, G. A retrospective analysis of health care costs for bone fractures in women with early-stage breast carcinoma. *Cancer* **2004**, *100*, 507–517.
10. Ghiasi, M.S.; Chen, J.; Vaziri, A.; Rodriguez, E.K.; Nazarian, A. Bone fracture healing in mechanobiological modeling: A review of principles and methods. *Bone Reports* **2017**.

11. Marsell, R.; Einhorn, T.A. The biology of fracture healing. *Injury* **2011**, *42*, 551–555.
12. Roberts, T.T.; Rosenbaum, A.J. Bone grafts, bone substitutes and orthobiologics: the bridge between basic science and clinical advancements in fracture healing. *Organogenesis* **2012**, *8*, 114–124.
13. Chan, J.K.; Glass, G.E.; Ersek, A.; Freidin, A.; Williams, G.A.; Gowers, K.; Santo, A.I.E.; Jeffery, R.; Otto, W.R.; Poulsom, R.; others. Low-dose TNF augments fracture healing in normal and osteoporotic bone by up-regulating the innate immune response. *EMBO molecular medicine* **2015**, p. e201404487.
14. Gaston, M.; Simpson, A. Inhibition of fracture healing. *Bone & Joint Journal* **2007**, *89*, 1553–1560.
15. Mountziaris, P.M.; Mikos, A.G. Modulation of the inflammatory response for enhanced bone tissue regeneration. *Tissue Engineering Part B: Reviews* **2008**, *14*, 179–186.
16. Wu, M.; Chen, G.; Li, Y.P. TGF-β and BMP signaling in osteoblast, skeletal development, and bone formation, homeostasis and disease. *Bone research* **2016**, *4*, 16009.
17. Kojouharov, H.V.; Trejo, I.; Chen-Charpentier, B.M. Modeling the effects of inflammation in bone fracture healing. *AIP Conference Proceedings* **2017**, *1895*, 020005.
18. Chung, E.; Son, Y. Crosstalk between mesenchymal stem cells and macrophages in tissue repair. *Tissue Engineering and Regenerative Medicine* **2014**, *11*, 431–438.
19. Schlundt, C.; Schell, H.; Goodman, S.B.; Vunjak-Novakovic, G.; Duda, G.N.; Schmidt-Bleek, K. Immune modulation as a therapeutic strategy in bone regeneration. *Journal of experimental orthopaedics* **2015**, *2*, 1.
20. Mantovani, A.; Sozzani, S.; Locati, M.; Allavena, P.; Sica, A. Macrophage polarization: tumor-associated macrophages as a paradigm for polarized M2 mononuclear phagocytes. *Trends in immunology* **2002**, *23*, 549–555.
21. Schmidt-Bleek, K.; Schell, H.; Lienau, J.; Schulz, N.; Hoff, P.; Pfaff, M.; Schmidt, G.; Martin, C.; Perka, C.; Buttgereit, F.; others. Initial immune reaction and angiogenesis in bone healing. *Journal of tissue engineering and regenerative medicine* **2014**, *8*, 120–130.
22. Doblaré, M.; Garcıa, J.; Gómez, M. Modelling bone tissue fracture and healing: a review. *Engineering Fracture Mechanics* **2004**, *71*, 1809–1840.
23. Border, W.A.; Noble, N.A. Transforming growth factor β in tissue fibrosis. *New England Journal of Medicine* **1994**, *331*, 1286–1292.
24. Cavaillon, J.M. Pro-versus anti-inflammatory cytokines: myth or reality. *Cellular and molecular biology (Noisy-le-Grand, France)* **2001**, *47*, 695–702.
25. Osta, B.; Benedetti, G.; Miossec, P. Classical and paradoxical effects of TNF-α on bone homeostasis. *Frontiers in immunology* **2014**, *5*, 48.
26. Arango Duque, G.; Descoteaux, A. Macrophage cytokines: involvement in immunity and infectious diseases. *Frontiers in immunology* **2014**, *5*, 491.
27. Gu, Q.; Yang, H.; Shi, Q. Macrophages and bone inflammation. *Journal of Orthopaedic Translation* **2017**.
28. Sherratt, J.A.; Murray, J. Models of epidermal wound healing. *Proc. R. Soc. Lond. B* **1990**, *241*, 29–36.
29. Serhan, C.N.; Savill, J. Resolution of inflammation: the beginning programs the end. *Nature immunology* **2005**, *6*, 1191–1197.
30. Newman, S.L.; Henson, J.E.; Henson, P.M. Phagocytosis of senescent neutrophils by human monocyte-derived macrophages and rabbit inflammatory macrophages. *Journal of Experimental Medicine* **1982**, *156*, 430–442.
31. Italiani, P.; Boraschi, D. From monocytes to M1/M2 macrophages: phenotypical vs. functional differentiation. *Frontiers in immunology* **2014**, *5*.
32. Wang, Y.; Yang, T.; Ma, Y.; Halade, G.V.; Zhang, J.; Lindsey, M.L.; Jin, Y.F. Mathematical modeling and stability analysis of macrophage activation in left ventricular remodeling post-myocardial infarction. *BMC genomics* **2012**, *13*, S21.
33. Bailon-Plaza, A.; Van Der Meulen, M.C. A mathematical framework to study the effects of growth factor influences on fracture healing. *Journal of Theoretical Biology* **2001**, *212*, 191–209.
34. Echeverri, L.; Herrero, M.; Lopez, J.; Oleaga, G. Early stages of bone fracture healing: formation of a fibrin–collagen scaffold in the fracture hematoma. *Bulletin of mathematical biology* **2015**, *77*, 156–183.
35. Einhorn, T.A. The science of fracture healing. *Journal of orthopaedic trauma* **2005**, *19*, S4–S6.
36. Einhorn, T.A.; Gerstenfeld, L.C. Fracture healing: mechanisms and interventions. *Nature Reviews Rheumatology* **2015**, *11*, 45.

37. Gómez-Barrena, E.; Rosset, P.; Lozano, D.; Stanovici, J.; Ermthaller, C.; Gerbhard, F. Bone fracture healing: cell therapy in delayed unions and nonunions. *Bone* **2015**, *70*, 93–101.
38. Nagaraja, S.; Wallqvist, A.; Reifman, J.; Mitrophanov, A.Y. Computational approach to characterize causative factors and molecular indicators of chronic wound inflammation. *The Journal of Immunology* **2014**, *192*, 1824–1834.
39. Yu, T. Design and validation of a mathematical model to describe macrophage dynamics in wound healing. PhD thesis, Drexel University, 2014.
40. Marée, A.F.; Komba, M.; Dyck, C.; Labkecki, M.; Finegood, D.T.; Edelstein-Keshet, L. Quantifying macrophage defects in type 1 diabetes. *Journal of theoretical biology* **2005**, *233*, 533–551.
41. Otto, S.P.; Day, T. *A biologist's guide to mathematical modeling in ecology and evolution*; Princeton University Press, 2011.
42. Isaksson, H. Recent advances in mechanobiological modeling of bone regeneration. *Mechanics Research Communications* **2012**, *42*, 22–31.
43. Van Furth, R.; Diesselhoff-den Dulk, M.M.; Mattie, H. Quantitative study on the production and kinetics of mononuclear phagocytes during an acute inflammatory reaction. *Journal of experimental medicine* **1973**, *138*, 1314–1330.
44. Schell, H.; Duda, G.; Peters, A.; Tsitsilonis, S.; Johnson, K.; Schmidt-Bleek, K. The haematoma and its role in bone healing. *Journal of experimental orthopaedics* **2017**, *4*, 5.
45. Lu, Y.; Lekszycki, T. Modeling of an initial stage of bone fracture healing. *Continuum Mechanics and Thermodynamics* **2015**, *27*, 851.
46. Hoegel, F.; Abdulazim, A.; Augat, P.; Buehren, V. Quantification of reaming debris at the fracture gap of diaphyseal A2 and A3 Fractures After reamed intramedullary nailing of the sheep tibia. *European Journal of Trauma and Emergency Surgery* **2008**, *34*, 587–591.
47. Recknagel, S.; Bindl, R.; Brochhausen, C.; Göckelmann, M.; Wehner, T.; Schoengraf, P.; Huber-Lang, M.; Claes, L.; Ignatius, A. Systemic inflammation induced by a thoracic trauma alters the cellular composition of the early fracture callus. *Journal of Trauma and Acute Care Surgery* **2013**, *74*, 531–537.
48. Gibon, E.; Loi, F.; Córdova, L.A.; Pajarinen, J.; Lin, T.; Lu, L.; Nabeshima, A.; Yao, Z.; Goodman, S.B. Aging affects bone marrow macrophage polarization: relevance to bone healing. *Regenerative engineering and translational medicine* **2016**, *2*, 98–104.
49. Stuart, A.; Humphries, A.R. *Dynamical systems and numerical analysis*; Vol. 2, Cambridge University Press, 1998.
50. Strang, G.; Strang, G.; Strang, G.; Strang, G. *Introduction to linear algebra*; Vol. 3, Wellesley-Cambridge Press Wellesley, MA, 1993.